Finite-size effects of correlation lengths in planar uniaxial ferromagnets

D. B. Abraham,[1] A. O. Parry,[2] and P. J. Upton[1,3,4]
[1]Department of Physics, Theoretical Physics, 1 Keble Road, Oxford 0X1 3NP, England
[2]Department of Mathematics, Imperial College of Science, Technology and Medicine, 180 Queen's Gate, London SW7 2BZ, England
[3]H. H. Wills Physics Laboratory, University of Bristol, Bristol BS8 1TL, England
[4]School of Theoretical Physics, Dublin Institute for Advanced Studies, 10 Burlington Road, Dublin 4, Ireland
(Received 6 September 1994)

The finite-size structure of two-point correlation functions is studied using the bubble model applied to the two-dimensional Ising model at subcritical temperatures in a small bulk field H wrapped around a cylinder with a circumference of M lattice sites. Particular emphasis is placed on a crossover occurring in the mass gap at $|H|=H_\times$ corresponding to an "avoided level crossing" in the second and third eigenvalues of the transfer matrix. It is argued that this crossover occurs because the class of bubble determining the behavior of correlation functions changes from a single connected closed loop for $|H|>H_\times$ to two disconnected closed loops encircling the cylinder for $0<|H|<H_\times$. The differing structures of the two-point correlation functions when $0<|H|<H_\times$ as compared to $|H|>H_\times$ are also determined using the bubble model. It is found that at a subcritical temperature T, the correlation length ξ for $0<|H|<H_\times$ is given by $1/\xi=2mHM/k_BT$, where m is the magnetization, and for $|H|>H_\times$ it is given by $1/\xi=2\tau+\alpha|H|^{2/3}$, where τ is the interfacial tension in units of k_BT and $\alpha>0$ is some temperature-dependent coefficient. Previous analysis of the transfer matrix by Privman and Schulman [J. Phys. A **15**, L231 (1982) and J. Stat. Phys. **29**, 205 (1982)] suggested that $H_\times \propto M^{-1}$, which was then further refined by Privman and Fisher [J. Stat. Phys. **33**, 385 (1983)], who claimed that $H_\times=k_BT\tau/mM$. This is confirmed here by the bubble model to leading order for large M but with additive algebraic corrections—the first two going like $M^{-5/3}$ and $M^{-7/3}$. At $H=0$, the class of bubble determining the behavior of the pair-energy-density correlation function is found to be that of a single closed connected loop similar to the case when $|H|>H_\times$ but with greater symmetry due to having $H=0$. It is shown that the effect of this greater symmetry can be understood from topological considerations of the allowed loop configurations.

PACS number(s): 05.50.+q, 64.60.Fr, 75.10.Hk, 03.65.−w

I. INTRODUCTION

In this paper, we shall concern ourselves with the behavior of two-point correlation functions (pair spin and pair energy density) in planar Ising-like models wrapped on cylinders of infinite length but finite circumference M (in units of lattice spacing). Specifically, we shall keep the temperature T below that of the critical point T_c and have a bulk field H that will usually be kept nonzero. In the limit of infinite M and for small H, this is, of course, in the vicinity of the first-order phase boundary—for finite M, models of this kind have been studied extensively with the view of understanding (a) finite-size scaling and rounding of first-order phase transitions [1] and (b) essential singularities on the phase boundary [2–5].

Particular attention has been paid to the structure of the spectrum of the subcritical planar-Ising transfer matrix as a function of H [1–5]. Consider the so-called "free-energy levels" defined by

$$f_n(H,T;M)=-(\beta M)^{-1}\ln\Lambda_n(H,T;M) \tag{1.1}$$

for $n=0,1,2,\ldots$, where $\beta=1/k_BT$ and Λ_n are the eigenvalue Λ_0 and $\Lambda_0>\Lambda_1>\Lambda_2\cdots$. Thus, in the limit $M\to\infty$, the free-energy density is $f_0(H,T;\infty)$. If $\mathcal{O}(X,Y)$ is a lattice operator (e.g., a spin or bond energy) at site (X,Y) on the Ising lattice (with the X direction running parallel to the cylinder axis) then the truncated pair-correlation function decays asymptotically like

$$\begin{aligned}\langle\mathcal{O}(0,0)\mathcal{O}(X,0)\rangle^T&\equiv\langle\mathcal{O}(0,0)\mathcal{O}(X,0)\rangle\\&\quad-\langle\mathcal{O}(0,0)\rangle\langle\mathcal{O}(X,0)\rangle\\&\sim\exp[-X/\xi(H,T;M)]\end{aligned} \tag{1.2}$$

as $X\to\infty$ (ignoring prefactors for the time being). Here X (and Y) is measured in units of lattice spacing. The correlation length is given by

$$1/\xi(H,T;M)=\beta M(f_1-f_0) \tag{1.3}$$

provided the relevant matrix element is nonzero [6].

The first three free-energy levels are plotted schematically against H in Fig. 1. Here we follow Privman and Fisher [1], who brought together information gained from a variety of studies—rigorous results for $H=0$ and $T\geq 0$ [7] and rigorous results for $T=0$ and $H\neq 0$ [5]—together with a more general analysis for $T>0$ and $H\neq 0$ such as, in particular, that of Privman and Schulman [4,5]. Clearly, by spin-inversion symmetry, Fig. 1 is symmetrical about $H=0$. We now describe some of its salient features.

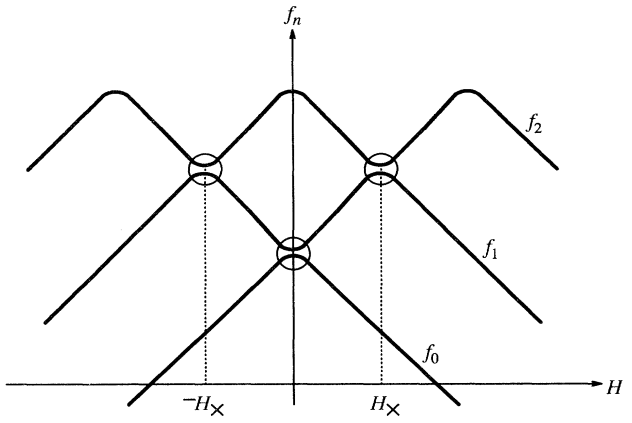

FIG. 1. Schematic plots of the first three "free-energy levels," i.e., $f_n=-(\beta M)^{-1}\ln\Lambda_n$ for $n=0,1,2$, as a function of the bulk field H, for the two-dimensional Ising model on a cylinder with M lattice sites along its circumference. The circles denote the "avoided-level-crossing" regions, which are *exponentially* small in M. *Not* shown here are the "multiparticle" bands lying above f_2 at $H=0$, which extend into $H\neq 0$ for $|H|<H_\times$, and the "single-particle" bands lying between f_1 and f_2 for $|H|>H_\times$.

(i) At $H=0$, the first two levels f_0 and f_1 are asymptotically degenerate [8] such that as $M\to\infty$

$$f_1-f_0\sim e^{-\tau M}\ , \tag{1.4}$$

where we ignore prefactors and τ is the interfacial tension divided by k_BT. The region of "avoided level crossing," where f_0 and f_1 are separated as in (1.4), is believed [2] to continue for nonzero H up to $|H|\sim\exp(-\tau M)$.

(ii) Asymptotic degeneracy is also present at $H=H_\times$ for f_1 and f_2 (see Fig. 1). Here, following Newman and Schulman [2], it is assumed that $f_2-f_1\sim\exp(-cM)$, where now c may be H dependent and that the avoided-level-crossing region, centered on $H_\times$, is also of order $\exp(-cM)$, in analogy with (i).

(iii) For small $|H|<H_\times$, but outside the avoided-level-crossing region, and M large, we have that $\partial f_0/\partial H\approx -m^*\mathrm{sgn}(H)$, where $m^*>0$ is the spontaneous magnetization [9] and, from level-crossing ideas [2], $\partial f_1/\partial H\approx +m^*\mathrm{sgn}(H)$.

(iv) Level-crossing ideas analogous to those in (iii) can be employed near $H_\times$. Thus, outside the region of avoided level crossing, the slope of f_2 (f_1) for H just above $H_\times$ is equal to that of f_1 (f_2) for H just below $H_\times$.

(v) For $H=0$ and for large M,

$$f_2-f_1\approx 1/\beta M\xi_\infty(T)\ , \tag{1.5}$$

where $\xi_\infty(T)$ is the correlation length of a single bulk phase [7].

(vi) For sufficiently small $H>H_\times$ and large M, the correlation length $\xi(H,T;M)$, given by (1.3), can be taken to be approximately $\xi_\infty(T)$ as given by (1.5) [1].

(vii) Above f_2 for $H=0$, there exists a band of "two-particle" states. Successive levels making up this band have a separation of the order of $1/M^3$ for large M, or, in other words, successive values of $\ln\Lambda_n$ in this band differ by an amount going like $1/M^2$. These form "single-particle bound pairs" for $H\neq 0$ [10] [see (viii) below]. This band is not depicted in Fig. 1.

(viii) Between f_1 and f_2 for $H>H_\times$, there exists a band of single-particle states [10] (again, not shown in Fig. 1). In the limit $M\to\infty$, levels making up this band have a separation going like $H^{2/3}$ for small H, this being related to the McCoy-Wu "mass" spectrum [11]. More will be said about this later.

From the above properties, Privman and Fisher [1] were able to predict heuristically the value of $H_\times$ through the following argument. If one assumes that f_0, f_1, and f_2 are piecewise linear functions of H with slopes given by $\pm m^*$ in accordance with properties (iii)–(vi) (reasonable since the regions of avoided level crossing are exponentially small in M for large M), then

$$f_2(H=0,T)-m^*H_\times=f_1(H=0,T)+m^*H_\times \tag{1.6}$$

from which, using (1.5), it follows immediately that $H_\times$ is given by

$$\frac{2m^*H_\times}{k_BT}=\frac{1}{M\xi_\infty(T)}\ . \tag{1.7}$$

This result is known to be true in the limit $T\to 0$ [4,5] and is believed to hold for general $T<T_c$. It was important for Privman and Fisher [1] to assess the size of $H_\times$ since one of the main themes of their paper was to investigate finite-size rounding of the first-order phase transition by an approximation to the partition function, which only takes into account the first two eigenvalues Λ_0 and Λ_1 of the transfer matrix. This procedure can only be justified for $H\ll H_\times$, where f_0 and f_1 are much closer to one another than either are to f_2.

Note also that, under the same assumptions leading to (1.7), for $H<H_\times$ we have that $f_1-f_0=2m^*H$ and hence, by (1.3), the correlation length is given by $1/\xi(H,T;M)=2m^*H\beta M$ whereas $1/\xi(H,T;M)=1/\xi_\infty(T)$ for $H>H_\times$. Thus $H_\times$ marks a crossover between two regimes with very different behavior in the correlation function. The main purpose of this paper is to investigate this crossover from a different point of view, one that does not require knowledge of the transfer-matrix spectrum, but which enables us to predict in greater detail the full structure of the correlation function for these two regimes.

Here we apply the "bubble model" for correlation functions [12,13], which is developed in detail in Sec. II. Two types of bubble, shown in Fig. 2, incorporating the important fluctuations, contribute to the two-point function—one type will dominate for $0<H<H_\times$ [Fig. 2(i)] while the other will control behavior for $H>H_\times$ [Fig. 2(ii)]. The bubbles delineate regions of reversed magnetization so that at the crossover point, given by equality of free-energy fluctuations, we have $2\beta m^*H_\times MX=X/\xi_\infty(T)$, which is (1.7). In Sec. III the bubble model is evaluated for $0<H<H_\times$, predicting the

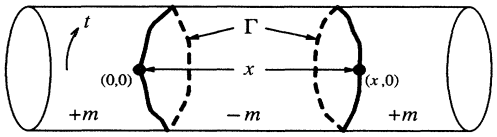

(i)

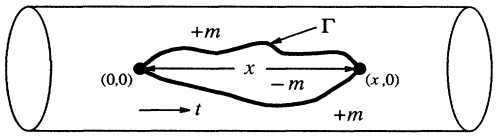

(ii)

FIG. 2. Two types of bubble Γ, separating domains of opposite magnetization $\pm m$, giving leading-order contributions to the two-point function $u_2(x)$. (i) shows a bubble of type $\mathcal{A}$, where Γ splits into two disconnected closed loops with each winding around the cylinder; (ii) shows a bubble of type $\mathcal{B}$, where Γ stays as a single connected closed loop. In the functional-integral evaluation of $u_2(x)$, which treats Γ as particle world lines, the timelike direction is indicated by the t arrows—one going around the cylinder in (i) and the other pointing along the cylinder axis in (ii).

form of the correlation function in this regime. Some details of the asymptotic analysis used here are left to the Appendix. In Sec. IV we evaluate the model for the other type of bubble, thus determining the behavior of the two-point function for $H > H_\times$. The results of Secs. III and IV are brought together in Sec. V, giving rise to a more precise prediction for $H_\times$ involving additive corrections to (1.7) that are algebraic in M. In Sec. VI we apply the bubble model to the pair-energy-density correlation function directly at $H=0$ with emphasis on differences occurring due to the absence of broken symmetry for this case as compared to when $H>0$. We finish with a conclusion in Sec. VII.

II. BUBBLE MODEL

The bubble model was introduced to describe subcritical ($T < T_c$) correlation functions [12,13] and is known to give reliable information on the asymptotic behavior of two-point correlation functions for all $T < T_c$ and small $|H|$, i.e., close to the phase boundary [12–16]. The basic idea is to suppose that after coarse graining to length scales of the order of the bulk correlation length ξ_∞, the important configurations contributing to $\langle \mathcal{O}(0,0)\mathcal{O}(X,Y)\rangle^T$ will be self-avoiding simple-closed loops Γ or bubbles, passing through the two points (0,0) and (X,Y) being correlated. Loops that pass through one point but not the other or Γ consisting of two disconnected loops, each of which is rooted at either (0,0) or (X,Y), are not counted since these will contribute to the disconnected part of $\langle \mathcal{O}(0,0)\mathcal{O}(X,Y)\rangle$ and are thus removed by truncation of the one-point functions in the definition of $\langle \mathcal{O}(0,0)\mathcal{O}(X,Y)\rangle^T$ in (1.2). The connected simple-closed nature of Γ supposes that we are correlating on a simply connected space such as an infinite plane (the focus of most previous bubble-model work [12–16]) or finite-width strips with boundary fields [17]. This supposition will no longer hold in the case of the cylinder considered here, as will be explained later. The loop Γ will carry an interfacial tension τ and enclose domains of opposite magnetization (equal magnitude, opposite sign) with the magnetization outside the loop being determined by either a condition on the boundary of the lattice or, in the case of interest to this paper, the presence of a bulk symmetry-breaking magnetic field. The two-point function can then be written as a sum over the bubble configurations Γ

$$\langle \mathcal{O}(0,0)\mathcal{O}(X,Y)\rangle^T = U_0 \sum_\Gamma e^{-\beta E(\Gamma)} , \tag{2.1}$$

where the "effective" energy of the loop Γ is given by

$$E(\Gamma) = \beta^{-1}\tau l(\Gamma) + 2mH A(\Gamma) , \tag{2.2}$$

where $l(\Gamma)$ is the length of Γ and $A(\Gamma)$ is the area enclosed by Γ. Since H is assumed to be small, the magnetization m is usually taken to be at its spontaneous value m^*. The prefactor U_0 is m^2 for the pair-spin-correlation function and $4\tau^2$ for the pair-energy-density function [16]. At this stage it is worth stressing that the bubble model could describe more general situations where the order parameter has O(1) symmetry, not just the Ising model, although in what follows we shall restrict ourselves to this case.

In all that follows, we shall redefine all distances to be in units of $1/\tau$ so that the correlation coordinates are $x=\tau X$, $y=\tau Y$ and the cylinder circumference is now $L=\tau M$. We shall also use the scaled field variable

$$h = \frac{2mH}{\tau^2 k_B T} , \tag{2.3}$$

which will be kept positive [18]. Hence we now denote $\langle \mathcal{O}(0,0)\mathcal{O}(X,0)\rangle^T$ by $u_2(x)$ and $\beta E(\Gamma)$ becomes simply $\beta E(\Gamma) = l(\Gamma) + h A(\Gamma)$, now that all lengths are measured in units of $1/\tau$, so that

$$u_2(x) = U_0 \sum_\Gamma \exp\{-[l(\Gamma) + h A(\Gamma)]\} . \tag{2.4}$$

Two types of bubble contributing to $u_2(x)$ for finite L are illustrated in Fig. 2. What we shall call type $\mathcal{A}$ is shown in Fig. 2(i), where the bubble Γ breaks up into two *disconnected* loops, with each one winding round the cylinder and pinned to one of the correlation points. The two loops will be coupled by the action of the field h since for this case $A(\Gamma)$ is the area of the region between the two loops making up Γ. The other class of bubble, type $\mathcal{B}$, stays as a single *connected* simple-closed loop and is shown in Fig. 2(ii). Disconnected bubbles that do *not* wrap around the cylinder do not occur in (2.4) because they are already taken into account in the one-point function parts.

As $x \to \infty$ and h sufficiently small but *nonzero,* type $\mathcal{A}$ bubbles dominate since they have a lower $E(\Gamma)$ than those of type $\mathcal{B}$. This situation changes as h increases until, eventually, type $\mathcal{B}$ bubbles dominate. If Γ_0 is the minimal-energy bubble (i.e., Wulff shape [19]), then for type $\mathcal{A}$, $\beta E(\Gamma_0) \approx 2L + hLx$, whereas for type $\mathcal{B}$, $\beta E(\Gamma_0) \approx 2x$. Hence, as $x \to \infty$

$$u_2(x) \sim \begin{cases} e^{-hLx} & \text{for } 0 < h < h_\times \text{ (type } \mathcal{A}) \\ e^{-2x} & \text{for } h > h_\times \text{ (type } \mathcal{B}) , \end{cases} \tag{2.5}$$

where the "crossover" field $h_\times$ is given by

$$h_\times = 2/L , \tag{2.6}$$

in exact agreement with (1.7) but now written in terms of scaled variables [note that when comparing with (1.7) one needs to use $\tau \xi_\infty = \frac{1}{2}$]. Thus we arrive at a simple physical mechanism behind the crossover behavior seen in the transfer-matrix spectrum.

For the type $\mathcal{A}$ case, one might have worried about domain configurations consisting of further loops winding round the cylinder in addition to the two passing through the correlation points, i.e., Γ as shown in Fig. 2(i). However, these can be discounted by the following argument. Since $h > 0$, the magnetization in the domain outside Γ is positive. Therefore, only an even number of additional loops can form within Γ. If two were to form, one would be pulled by the action of the field h towards the loop passing through (0,0) and the other would be similarly pulled to the loop passing through $(x,0)$. This will behave as though $h=0$ (see below) but with L replaced by $2L$ (coming from two loops passing through each correlation point). After truncation of the part that remains in $u_2(x)$ after the limit $x \to \infty$ is taken, this configuration gives a contribution to $u_2(x)$ going like $\exp(-x^2/2L)$ and thus highly subdominant to the simpler two-loop configuration Γ (type $\mathcal{A}$) shown in Fig. 2(i).

The average distance separating the upper and lower sides of Γ for the type $\mathcal{B}$ bubble [see Fig. 2(ii)] is proportional to $h^{-1/3}$ for large L and x. This is because the boundary of the type $\mathcal{B}$ bubble separates phases that do not coexist since $H \neq 0$. If we treat the phase inside the bubble as if it sits on a substrate, we have a wetting problem, the solution of which is already known [20,21]. Then $h \langle A(\Gamma) \rangle \propto h^{2/3} x$, leading to a form for $u_2(x)$ for $h > h_\times$ consistent with McCoy and Wu [11]. This will give an algebraic correction of $O(L^{-5/3})$ to the right-hand side of (2.6). A fuller discussion of this will be left to Sec. V.

Finally, we stress that our analysis will usually be confined to $h > 0$. We will certainly have nothing to say about asymptotic degeneracy at $h=0$ and $h_\times$. However, at this stage, it should be noted that although type $\mathcal{A}$ bubbles dominate over type $\mathcal{B}$ for $0 < h < h_\times$, they do *not* do so at $h=0$. It will be shown in the Sec. VI that $u_2(x) \sim \exp(-x^2/L)$ for type $\mathcal{A}$ bubbles at $h=0$ (after truncating away additive x-independent terms), which is *highly* subdominant to $u_2(x) \sim \exp(-2x)$ as determined from type $\mathcal{B}$ bubbles at $h=0$. Indeed, a recent study of pair-energy-density correlation functions on cylinders at $h=0$ was conducted where an *exact* Ising analysis was shown to compare quite well with the bubble model using type $\mathcal{B}$ bubbles [22]. Pair-energy-density correlation functions are not, of course, affected by asymptotic degeneracy at $h=0$, unlike pair-spin-correlation functions.

In the following two sections, functional integration techniques are used to evaluate the bubble model for $u_2(x)$ more quantitatively, with type $\mathcal{A}$ bubbles in Sec. III and type $\mathcal{B}$ bubbles left to Sec. IV. We shall use the notation $u_2(x|\mathcal{A})$ and $u_2(x|\mathcal{B})$ to denote the contribution to $u_2(x)$ coming from bubbles of type $\mathcal{A}$ and type $\mathcal{B}$, respectively.

III. EVALUATION OF TYPE $\mathcal{A}$ BUBBLES

We evaluate Eq. (2.4) by limiting to a functional integral that can be regarded as a quantum-mechanical propagator in Euclidean time [14,15,22,23]. For type $\mathcal{A}$ bubbles, it is convenient to treat the direction perpendicular to the cylinder axis, that is, the y direction, as the timelike (t) direction—this is indicated by the t arrow in Fig. 2(i). The two loops forming Γ are allowed to fluctuate in the x direction with a solid-on-solid (SOS) constraint (no overhangs) applied to the timelike y direction. One then treats the loops as world lines for two particles $x_1(t)$ and $x_2(t)$, shown schematically in Fig. 3, with initial positions at $x_1(0)=0$ and $x_2(0)=x$ and final positions at $t=L$ satisfying $x_j(L)=x_j(0)$ for $j=1,2$, since, of course, each loop closes on itself. The length of the world line for particle $j=1,2$ is

$$l_j(\Gamma) = \int_0^L \sqrt{1+\dot{x}_j^2}\, dt , \tag{3.1}$$

where throughout this paper we use $\dot{x}_j = dx_j/dt$. We shall adopt the nonrelativistic approximation

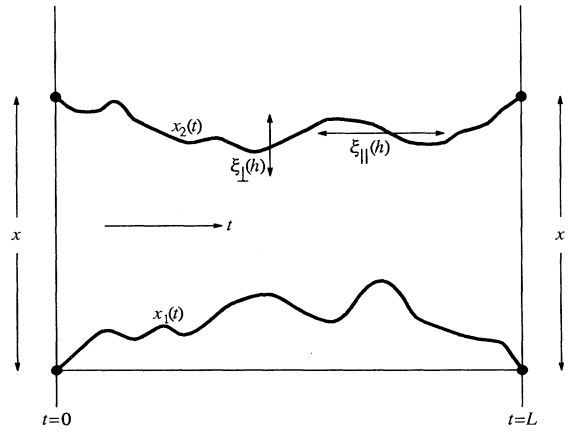

FIG. 3. Two world lines $x_1(t)$ and $x_2(t)$ for a type $\mathcal{A}$ bubble, obtained from rolling the cylinder out at the seam joining $y=0$ with $y=L$ so that the world lines start at $t=0$ and end at $t=L$. Their characteristic length scales parallel and perpendicular to the y axis (t direction) are denoted schematically by $\xi_\parallel(h)$ and $\xi_\perp(h)$, respectively.

$\sqrt{1+\dot{x}_j^2}\approx 1+\dot{x}_j^2/2$ so that Eq. (2.4) can be expressed in terms of a quantum-mechanical propagator, for two *noncrossing* nonrelativistic particles of unit mass interacting through a linear potential, as

$$u_2(x|\mathcal{A})=U_0\int_{x_1(0)=0,x_2(0)=x}^{x_1(L)=0,x_2(L)=x}[dx_1dx_2]\times\exp(-S_2[x_1,x_2])\ , \tag{3.2}$$

where the Euclidean action is

$$S_2[x_1,x_2]=2L+\int_0^L dt\{\tfrac{1}{2}\dot{x}_1^2+\tfrac{1}{2}\dot{x}_2^2+h(x_2-x_1)\}\ . \tag{3.3}$$

The measure in (3.2) is over all noncrossing paths with $x_2(t)\geq x_1(t)$ satisfying the indicated initial and final conditions. It is known that by rescaling distances in units of $1/\tau$, no additional scale factors are needed in the measure [23].

One can easily evaluate (3.2) by going over to "center of mass" $x_+(t)$ and "relative" $x_-(t)$ coordinates defined through

$$x_\pm(t)=\frac{1}{\sqrt{2}}(x_2\pm x_1)(t) \tag{3.4}$$

so that (3.2) becomes

$$u_2(x|\mathcal{A})=U_0e^{-2L}K_+(L)K_-(x;L)\ , \tag{3.5}$$

where $K_+(L)$ is the propagator for the center-of-mass motion

$$K_+(L)=\int_{x_+(0)=x_+(L)}[dx_+]\exp\left[-\int_0^L\tfrac{1}{2}\dot{x}_+^2dt\right] \tag{3.6}$$

with the measure over world lines having $x_+(t)\in(-\infty,\infty)$ while the propagator for the relative motion is

$$K_-(x;L)=\int_{x_-(0)=x/\sqrt{2}}^{x_-(L)=x/\sqrt{2}}[dx_-]e^{-S[x_-]} \tag{3.7}$$

with its Euclidean action given by

$$S[x_-]=\int_0^L dt(\tfrac{1}{2}\dot{x}_-^2+\sqrt{2}hx_-) \tag{3.8}$$

and the measure in (3.7) is over all world lines with $x_-(t)\geq 0$ for all $t\in[0,L]$.

The propagator $K_+(L)$ is merely that of a free nonrelativistic particle on an infinite line where it is well known that

$$K_+(L)=\frac{1}{\sqrt{2\pi L}}\ . \tag{3.9}$$

On the other hand, $K_-(x;L)$ is the propagator for a particle moving on a half line in a linear potential. We shall evaluate it in the following two subsections, each describing differing viewpoints.

A. Spectral decomposition of $K_-(x;L)$

The propagator defined by (3.7) can be expressed in the usual spectral form

$$K_-(x;L)=\sum_n|\varphi_n(x/\sqrt{2})|^2e^{-LE_n}\ , \tag{3.10}$$

where the eigenfunctions $\varphi_n(x)$ for $x\geq 0$ are solutions of the Schrödinger equation

$$\left[-\frac{1}{2}\frac{d^2}{dx^2}+\sqrt{2}hx\right]\varphi_n(x)=E_n\varphi_n(x) \tag{3.11}$$

with eigenvalues E_n. The eigenfunctions satisfy the boundary conditions $\varphi_n(0)=0$ (leading to quantization) and $\lim_{x\to\infty}\varphi_n(x)=0$ and the normalization condition $\int_0^\infty|\varphi_n(x)|^2dx=1$. The solutions to Eq. (3.11) can be expressed in terms of the Airy function $\mathrm{Ai}(x)$ with $E_n=-a_nh^{2/3}$, where a_n is the nth zero of the Airy function $\mathrm{Ai}(a_n)=0$ for $n=1,2,\ldots$ and $0>a_1>a_2>\cdots$. Hence, from (3.10), the propagator becomes

$$K_-(x;L)=\sqrt{2}h^{1/3}\sum_{n=1}^{\infty}\frac{\mathrm{Ai}^2(h^{1/3}x+a_n)e^{h^{2/3}La_n}}{[\mathrm{Ai}'(a_n)]^2}\ , \tag{3.12}$$

where $\mathrm{Ai}'(x)=d\ \mathrm{Ai}(x)/dx$.

Note, in (3.12), how x is scaled by $h^{1/3}$ and the circumference L is scaled by $h^{2/3}$. This scaling is a consequence of the presence of two length scales due to interfacial fluctuations. It is known from the theory of complete wetting in planar models [20,21] that for an interface (in $1+1$ dimensions) in a bulk field h above the wetting temperature, the interfacial correlation length parallel to the interface $\xi_\parallel(h)$ grows like $\xi_\parallel(h)\sim h^{-2/3}$ and there is a characteristic length perpendicular to the interface $\xi_\perp(h)$ growing like $\xi_\perp(h)\sim h^{-1/3}$ so that $\xi_\parallel\sim\xi_\perp^2$. These length scales are shown schematically in Fig. 3 and the scaling in (3.12) is now completely natural.

Since we wish to investigate $u_2(x)$ for large x, verifying (2.5) for $0<h<h_\times$, one needs to understand the asymptotic behavior of Eq. (3.12) as $h^{1/3}x\to\infty$. This we do by limiting the sum in (3.12) to a Riemann integral, the asymptotics of which is analyzed using Laplace's method, which, it turns out, requires that $h^{2/3}L$ also be large. The details of this calculation are given in the Appendix—here we just present the result, which says that

$$K_-(x;L)\approx\frac{\exp[-(hLx-\frac{1}{12}h^2L^3)]}{\sqrt{2\pi L}} \tag{3.13}$$

as $h^{1/3}x\to\infty$, $h^{2/3}L\to\infty$ such that $x>hL^2/4$. This, of course, gives rise to the expected x dependence in $u_2(x)\sim\exp(-hLx)$ for large x when $0<h<h_\times$.

B. Semiclassical approximation and the Wulff construction

In addition to the required x dependence in (3.13), one also has an additional term in the exponential together with a prefactor. These terms have a natural interpretation, understood from the familiar semiclassical approximation to the path integral $K_-(x;L)$, in (3.7)—a method related to the WKB approximation in quantum mechanics. In the classical limit, the path integral is dominated by the classical trajectory which is the minimal extremum of the action. One then expands about this tra-

jectory, with Gaussian fluctuation coming first. From the point of view of statistical mechanics, this classical path is the Wulff shape—the minimal-free-energy shape as determined by the Wulff construction [19].

For the Euclidean action $S[x_-]$ given by (3.8), the classical trajectory $x_{\rm cl}(t)$ for $t\in[0,L]$ is given by

$$\left.\frac{\delta S}{\delta x_-}\right|_{x_-=x_{\rm cl}}=0\ , \tag{3.14}$$

satisfying boundary conditions $x_{\rm cl}(0)=x_{\rm cl}(L)=x/\sqrt{2}$, from which it follows that

$$x_{\rm cl}(t)=\frac{1}{\sqrt{2}}\{ht(t-L)+x\}\ , \tag{3.15}$$

as shown schematically in Fig. 4. The condition $x>hL^2/4$ is needed in order to keep $x_{\rm cl}(t)>0$ for all $t\in[0,L]$. This requirement, also given just after (3.13), was also needed in the previous spectral approach [see the Appendix, especially Eq. (A7)].

By setting $x_-(t)=x_{\rm cl}(t)+\eta(t)$, Eq. (3.7) now becomes

$$K_-(x;L)=e^{-S[x_{\rm cl}]}\int_{\eta(0)=0}^{\eta(L)=0}[d\eta]\exp\left[-\int_0^L\tfrac{1}{2}\dot\eta^2dt\right]\ , \tag{3.16}$$

where

$$S[x_{\rm cl}]=hLx-\tfrac{1}{12}h^2L^3 \tag{3.17}$$

and the measure is on the set of paths with $\eta(t)\geq -x_{\rm cl}(t)$ for $t\in[0,L]$. The path integral over η has the action of a free particle confined to a half line with a time-dependent boundary point $-x_{\rm cl}(t)$. Thus far, Eq. (3.16) follows exactly from (3.7)—the approximation starts in the treatment of the functional integral over η. Following the usual saddle-point method, one relaxes the restriction placed on the range of $\eta(t)$ by allowing η to take all values in $\mathbb{R}$ for all $t\in(0,L)$. This is certainly a good approximation for large values of x. Hence the path integral in (3.16) is approximately that of a free particle on $\mathbb{R}$ so that

$$\int_{\eta(0)=0}^{\eta(L)=0}[d\eta]\exp\left[-\int_0^L\tfrac{1}{2}\dot\eta^2dt\right]\approx\frac{1}{\sqrt{2\pi L}}\ . \tag{3.18}$$

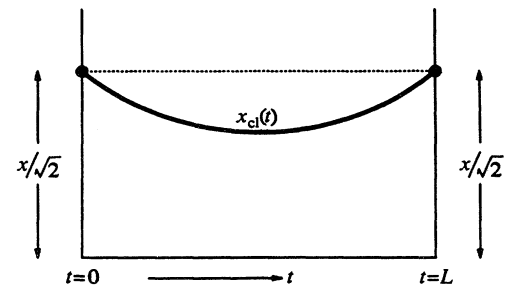

FIG. 4. Schematic depiction of the classical path (Wulff shape) $x_{\rm cl}(t)$ for the "relative" coordinate $x_-(t)$ of the type $\mathcal{A}$ bubble. Note how it sags towards the base line due to the effect of the bulk field.

Putting (3.17) and (3.18) into (3.16) gives (3.13) as required.

Note that $x_{\rm cl}(t)$ is the Wulff shape for the relative coordinate $x_-(t)$ with a free energy given by $S[x_{\rm cl}]$ in (3.17). If the Wulff shape consisted of straight lines, $x_{\rm cl}(t)=x/\sqrt{2}$ for all $t\in[0,L]$, then only the first term on the right-hand side of (3.17) would be included. The second term is a consequence of the tendency for the two loops forming Γ to bend together due to the effect of the field h, leading to a parabolic Wulff shape for the relative coordinate (see Fig. 4).

IV. EVALUATION OF TYPE $\mathcal{B}$ BUBBLES

In order to evaluate Eq. (2.4) for type $\mathcal{B}$ bubbles, using the functional integral approach as before, one now takes the cylinder axis (x direction) as the Euclidean timelike (t) direction and allow the bubble sides to fluctuate in the y direction with the SOS constraint applied to the x direction (see Fig. 2). Hence, again using the nonrelativistic approximation for the lengths of the "world lines" forming Γ, we have

$$u_2(x|\mathcal{B})=U_0\int_{y_1(0)=0,y_2(0)=y_0}^{y_1(x)=0,y_2(x)=y_0}[dy_1dy_2]\times\exp(-S_2[y_1,y_2])\ , \tag{4.1}$$

where $y_1(t)$ and $y_2(t)$ are the y displacements of, respectively, the lower and the upper sides of Γ for $0\leq t\leq x$. The measure is on the set of all noncrossing paths lying on the cylinder and having $y_2(t)\geq y_1(t)$ for all $t\in[0,x]$ with, as indicated, an initial and a final separation given by y_0. The value of y_0 is determined by comparison to the exact solution of the planar Ising model for $h=0$ [14–16,22]. So as to get the correct prefactors of the two-point correlation functions, it is required that $y_0=\frac{1}{2}$. The fact that y_0 is of order unity is physically reassuring. The two-particle Euclidean action $S_2[y_1,y_2]$ is given by

$$S_2[y_1,y_2]=2x+\int_0^x dt\{\tfrac{1}{2}\dot y_1^2+\tfrac{1}{2}\dot y_2^2+h(y_2-y_1)\}\ , \tag{4.2}$$

where, as usual, $\dot y_j=dy_j/dt$.

The particles cannot pass through one another and are confined to lie on a circle of circumference L so that the system is periodic under the mapping

$$P:\ (y_1,y_2)\mapsto(y_1+L,y_2+L)\ . \tag{4.3}$$

As in the previous section, (4.1) is factorized by separating into center of mass and relative coordinates through the transformation

$$y_\pm(t)=\frac{1}{\sqrt{2}}(y_2\pm y_1)(t)\ . \tag{4.4}$$

For a given y_2, y_1 is restricted, under the noncrossing and geometrical constraints, to satisfy $y_2-L\leq y_1\leq y_2$ and, in order that configurations are not repeated, y_2 must lie in an interval of length L by, for example, having $y_2\in[0,L]$. This gives a rather cumbersome parallelogram-shaped domain of integration in the

(y_1,y_2) plane, although this can be translated in the (1,1) direction under the periodicity mapping P. When rotating to the $y_\pm$ coordinates through (4.4), this periodicity can be exploited so that the domain of integration in the (y_+,y_-) plane becomes a simple rectangle having $0\le y_+\le\sqrt{2}L$ and $0\le y_-\le L/\sqrt{2}$ with periodicity under $y_+\mapsto y_++\sqrt{2}L$. In other words, the center-of-mass coordinate y_+ is that of a particle on a circle of circumference $\sqrt{2}L$ and the relative coordinate y_- is for a particle confined to a strip of width $L/\sqrt{2}$. One should note the role of periodicity in this coordinate decomposition, which would not have been possible for, say, two particles on a strip of finite width but with free edges.

Equation (4.1) can now be factorized, yielding

$$u_2(x|\mathcal{B})=U_0e^{-2x}K_+(x;L)K_-(x;L) \tag{4.5}$$

for which $K_+(x;L)$ is the propagator for the center-of-mass motion

$$K_+(x;L)=\int_{y_+(0)=y_+(x)}[dy_+]\exp\left[-\int_0^x\tfrac{1}{2}\dot{y}_+^2dt\right], \tag{4.6}$$

where the measure is over the set of paths $y_+(t)$ for $t\in[0,x]$, on a cylinder of circumference $\sqrt{2}L$, and the propagator for the relative-coordinate motion is

$$K_-(x;L)=\int_{y_-(0)=y_0/\sqrt{2}}^{y_-(x)=y_0/\sqrt{2}}[dy_-]\exp\left\{-\int_0^x dt(\tfrac{1}{2}\dot{y}_-^2+\sqrt{2}hy_-)\right\}, \tag{4.7}$$

with its measure being over the set of paths confined to the strip $0\le y_-(t)\le L/\sqrt{2}$ for $t\in[0,x]$.

A. Center-of-mass motion

The propagator $K_+(x;L)$ in (4.6) can be written in spectral form

$$K_+(x;L)=\sum_n|\varphi_n^+(y_0/\sqrt{2})|^2e^{-xE_n^+}, \tag{4.8}$$

where $\varphi_n^+(y_+)$ are the eigenstates satisfying

$$-\frac{1}{2}\frac{d^2}{dy_+^2}\varphi_n^+(y_+)=E_n^+\varphi_n^+(y_+) \tag{4.9}$$

with periodicity $\varphi_n^+(y_++\sqrt{2}L)=\varphi_n^+(y_+)$. Hence, after normalizing with

$$\int_0^{\sqrt{2}L}|\varphi_n^+(y_+)|^2dy_+=1, \tag{4.10}$$

we have

$$\varphi_n^+(y_+)=(\sqrt{2}L)^{-1/2}\exp(i\omega_n^+y_+), \tag{4.11}$$

where $\omega_n^+=n\pi\sqrt{2}/L$ for $n=0,\pm1,\pm2,\ldots$, with $E_n^+=\frac{1}{2}(\omega_n^+)^2$, so that

$$K_+(x;L)=\frac{1}{\sqrt{2}L}\sum_{n=-\infty}^{\infty}e^{-n^2\pi^2x/L^2}. \tag{4.12}$$

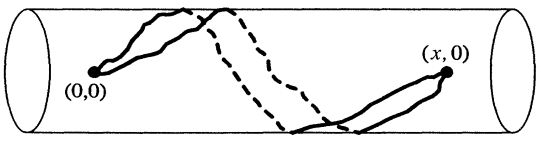

FIG. 5. Depiction of a type $\mathcal{B}$ bubble winding around the cylinder with a winding number of $n=1$ in the "center-of-mass" coordinate.

Clearly, $K_+(x;L)\approx1/\sqrt{2}L$ as $x\to\infty$. From the Poisson summation formula, (4.12) can be rewritten as

$$K_+(x;L)=\frac{1}{\sqrt{2\pi x}}\sum_{n=-\infty}^{\infty}e^{-n^2L^2/x}, \tag{4.13}$$

where the $n=0$ term, the only term surviving after the limit $L\to\infty$ is taken, is the propagator for a free particle on $\mathbb{R}$. Contributions due to finite L (higher n terms) can be interpreted as coming from bubbles that wind around the cylinder—the n in (4.13) corresponds to the "winding number" of the center of mass of the bubble. A bubble with winding number $n=1$, for example, is shown in Fig. 5. A fuller discussion of the role of topology and universal covering space ideas to the finite-size structure of correlation functions on cylinders was given in Ref. [22], but only for the case of the pair-energy-density correlation function when $h=0$. Here, where h is *strictly nonzero,* the two sides of the bubble must wind around together as a pair.

B. Relative-coordinate motion

As before, the propagator $K_-(x;L)$ in (4.7), being that of a quantum-mechanical particle in a linear potential confined to a strip of width $L/\sqrt{2}$, can be written

$$K_-(x;L)=\sum_{n=1}^{\infty}|\varphi_n^-(y_0/\sqrt{2})|^2e^{-xE_n^-}, \tag{4.14}$$

where now $\varphi_n^-(y_-)$ are eigenstates of the Schrödinger equation

$$\left[-\frac{1}{2}\frac{d^2}{dy_-^2}+\sqrt{2}hy_-\right]\varphi_n^-(y_-)=E_n^-\varphi_n^-(y_-) \tag{4.15}$$

with boundary conditions $\varphi_n^-(0)=\varphi_n^-(L/\sqrt{2})=0$ (coming from the noncrossing restriction) and with normalization

$$\int_0^{L/\sqrt{2}} |\varphi_n^-(y_-)|^2 dy_- = 1 \ . \tag{4.16}$$

In presenting the results, we write $E_n^- = E_n^-(h;L)$ in scaling form

$$E_n^-(h;L) = h^{2/3} M_n(h^{1/3}L) \tag{4.17}$$

for $n=1,2,\ldots$, where the scaling functions $M_n(z)$ are roots of the quantization condition

$$\mathrm{Ai}(-M_n)\mathrm{Bi}(z-M_n) = \mathrm{Bi}(-M_n)\mathrm{Ai}(z-M_n) \tag{4.18}$$

with $\mathrm{Bi}(z)$ being the Airy function of the second kind in standard notation [24]. We shall use the convention that $E_1^- < E_2^- < E_3^- < \cdots$. The eigenfunctions are given in terms of $z = h^{1/3}L$ by

$$\begin{aligned}\varphi_n^-(y_-) = {} & \frac{(\sqrt{2}h^{1/3})^{1/2}\pi \mathrm{Bi}(z-M_n(z))}{[\mathrm{Bi}^2(z-M_n(z)) - \mathrm{Bi}^2(-M_n(z))]^{1/2}} \\ & \times \{\mathrm{Ai}(-M_n(z))\mathrm{Bi}(\sqrt{2}h^{1/3}y_- - M_n(z)) \\ & - \mathrm{Bi}(-M_n(z))\mathrm{Ai}(\sqrt{2}h^{1/3}y_- - M_n(z))\} \ .\end{aligned} \tag{4.19}$$

Putting (4.17)–(4.19) into (4.14) gives the full expression for $K_-(x;L)$. Notice, from (4.17), that now x is scaled by $h^{2/3}$ and L (and y_0) is scaled by $h^{1/3}$—the opposite of the type $\mathcal{A}$ case described in Sec. III A. This is, of course, very natural since now, for type $\mathcal{B}$, the interfaces run along the cylinder axis with $\xi_\parallel(h) \sim h^{-2/3}$ being the length scale parallel to the interfaces (x direction) and $\xi_\perp(h) \sim h^{-1/3}$ the length scale perpendicular to the interfaces (y direction).

Now, for type $\mathcal{B}$ bubbles, the correlation function has the form

$$u_2(x|\mathcal{B}) = K_+(x;L) \sum_{n=1}^{\infty} p_n(h;L) e^{-m_n x} \ , \tag{4.20}$$

where $p_n(h;L) = U_0 |\varphi_n^-(y_0/\sqrt{2})|^2$ and the "single-particle masses" $m_n = m_n(h;L)$ are given by

$$m_n(h;L) = 2 + h^{2/3} M_n(h^{1/3}L) \ . \tag{4.21}$$

It follows from (4.18) that (see asymptotic formulas in Ref. [24])

$$M_n(z) \approx -a_n + \frac{\exp(-\frac{4}{3}z^{3/2})}{2\pi[\mathrm{Ai}'(a_n)]^2} + \cdots \tag{4.22}$$

as $z \to \infty$, where $\mathrm{Ai}(a_n) = 0$ with $0 > a_1 > a_2 > \cdots$ as before and from (4.19)

$$\lim_{h^{1/3}L \to \infty} \varphi_n^-(y_-) = \frac{(\sqrt{2}h^{1/3})^{1/2}\mathrm{Ai}(\sqrt{2}h^{1/3}y_- + a_n)}{\mathrm{Ai}'(a_n)} \ . \tag{4.23}$$

Hence, from (4.14), $\lim_{h^{1/3}L \to \infty} K_-(x;L)$ is identical to Eq. (3.12) after respectively substituting y_0 and x for x and L, which is, of course, as required.

The leading term in (4.22), substituted in (4.21), gives the usual McCoy-Wu mass spectrum [11] $m_n = 2 - a_n h^{2/3}$ for the infinite-size system. The scaling function $M_n(h^{1/3}L)$ describes how this mass spectrum is shifted due to the effect of the finite-size geometry.

V. DETERMINATION OF THE CROSSOVER FIELD

We are now in a position to give a more detailed prediction of the crossover field $H_\times$ in terms of $h_\times = 2mH_\times/\tau^2 k_B T$ than that obtained from the discussion leading to Eq. (2.6). To do this, we need to look at the large x behavior of $u_2(x)$.

From the results of Sec. III we have that

$$u_2(x) \approx \frac{U_0 \exp[-(2L + hLx - \frac{1}{12}h^2L^3)]}{2\pi L} \tag{5.1}$$

as $x \to \infty$ when only type $\mathcal{A}$ bubble contribute. On the other hand, when only type $\mathcal{B}$ bubbles are included, then, from the results of Sec. IV, as $x \to \infty$

$$u_2(x) \approx \frac{1}{\sqrt{2}L} \sum_{n=1}^{\infty} p_n(h;L) e^{-m_n x} \ , \tag{5.2}$$

where

$$p_n(h;L) = \frac{4^{-1}\sqrt{2}U_0 h \mathrm{Bi}^2(h^{1/3}L - M_n(h^{1/3}L))}{\mathrm{Bi}^2(h^{1/3}L - M_n(h^{1/3}L)) - \mathrm{Bi}^2(-M_n(h^{1/3}L))} \ , \tag{5.3}$$

with the masses $m_n = m_n(h;L)$ given in Eq. (4.21). Hence, comparing (5.1) with the leading term in (5.2), $h_\times$ is given by

$$\begin{aligned} h_\times L &= m_1(h_\times;L) \\ &= 2 + h_\times^{2/3} M_1(h_\times^{1/3}L) \ , \end{aligned} \tag{5.4}$$

with $u_2(x)$ given by (5.1) when $h < h_\times$ and (5.2) when $h > h_\times$.

Clearly, (5.4) implies that $h_\times \approx 2/L$ to leading order as before, but the $h_\times^{2/3}$ term will give rise to corrections to this that are algebraic in L. Now, from Remarks (i) and (ii) in the Introduction, the crossover region around $h_\times$ is expected to have a width that is *exponentially* small in L. It therefore makes sense to discuss algebraic shifts in the position of $h_\times$ for large L. Thus, by applying (4.22) to (5.4) and ignoring quantities exponentially small in L, we have

$$h_\times L \approx 2 - a_1 h_\times^{2/3} \tag{5.5}$$

for large L. This can be solved explicitly to yield

$$h_\times \approx \frac{2}{L} - \frac{a_1^3}{3L^3} + \frac{2^{1/3}a_1}{L^{5/3}} \left\{ \left[\left[1 - \frac{2a_1^3}{27L^2} \right]^{1/2} - 1 + \frac{a_1^3}{3L^2} - \frac{a_1^6}{54L^4} \right]^{1/3} - \left[\left[1 - \frac{2a_1^3}{27L^2} \right]^{1/2} + 1 - \frac{a_1^3}{3L^2} + \frac{a_1^6}{54L^4} \right]^{1/3} \right\}, \tag{5.6}$$

which incorporates the full algebraic dependence of $h_\times$ on L. By expanding (5.6) for large L we obtain leading algebraic corrections to $h_\times$ as

$$h_\times \approx \frac{2}{L} - \frac{2^{2/3}a_1}{L^{5/3}} + \frac{2^{4/3}a_1^2}{3L^{7/3}} + \cdots . \tag{5.7}$$

Corrections to Eq. (2.6) [and therefore (1.7)] of the form shown in (5.7) have not been anticipated by previous transfer-matrix studies.

VI. ZERO BULK FIELD

We now discuss the situation when $h=0$, where exact Ising results are available. This will enable us to compare the bubble model, evaluated at $h=0$, with the exact Ising model, but also we shall consider how the results of the previous sections in the limit of $h \to 0^+$ compare with the bubble model evaluated at $h=0$.

Throughout this section, we consider only the pair-energy-density correlation function whereas before, when $h \neq 0$, we were able to discuss *both* the pair-energy-density *and* the pair-spin-correlation functions within the bubble model. The reason why we do not discuss pair-spin-correlation functions using bubble-model ideas at $h=0$ is as follows. Recall that at $h=0$ there is asymptotic degeneracy in the eigenvalues of the transfer matrix as $L \to \infty$ for $T < T_c$. In particular, the two largest eigenvalues Λ_0 and Λ_1 coming from "vacuum" states are asymptotically degenerate, going like $\ln(\Lambda_0/\Lambda_1) \sim e^{-L}$ as $L \to \infty$ leading to the expression shown in (1.4). Both these eigenvalues contribute to the pair-spin-correlation function, since the relevant matrix element is nonzero at $h=0$, which then gives the leading behavior of the correlation function as $x \to \infty$ with correlation length $\xi \sim e^L$. This type of behavior, coming from the vacuum sector of the transfer matrix, cannot be picked up by the bubble model as applied in this paper, which was designed to describe the two-particle sector of the transfer matrix. However, the situation is very different for the pair-energy-density correlation function since for this case the matrix element joining Λ_0 and Λ_1 is *zero* at $h=0$ (see [6]) and indeed the complete expression for this correlation function is obtained in its entirety from the two-particle sector [22].

So far, we have argued that type $\mathcal{A}$ bubbles dominate over those of type $\mathcal{B}$ when h is sufficiently small but *nonzero*, i.e., $0 < h < h_\times$. However, in Sec. VI A, it will be demonstrated that at $h=0$ type $\mathcal{A}$ bubbles become *highly* subdominant and the pair-energy-density correlation function is described by bubbles of type $\mathcal{B}$. The behavior of type $\mathcal{B}$ bubbles at $h=0$ compared to the case when $h \to 0^+$, will be discussed in Sec. VI B. Here we shall also compare results to that of a strip of finite width at $h=0$ but with spins fixed to be up along both edges—again exactly soluble for the Ising model.

A. Type $\mathcal{A}$ bubbles

For type $\mathcal{A}$, $K_+(L)$ defined by (3.6) and given by (3.9) is, of course, independent of h and we need only consider $K_-(x;L)$ as defined by (3.7) with (3.8) for $h=0$. This could be obtained by taking the $h \to 0^+$ limit of (3.12), but it is just as simple to solve directly the time-dependent Schrödinger equation (diffusion equation) satisfied by the propagator $K(x,x_0;t)$ describing the evolution of a *free* particle with initial position at x_0 and final position at x after time t with the evolution confined to the half line $x \geq 0$. Thus we require the solution of

$$\left[\frac{\partial}{\partial t} - \frac{1}{2} \frac{\partial^2}{\partial x^2} \right] K(x,x_0;t) = 0 \tag{6.1}$$

for $x \geq 0$, with initial condition $K(x,x_0;0) = \delta(x - x_0)$ and a Dirichlet boundary condition $K(0,x_0;t) = 0$ since the particle cannot cross $x=0$. Hence, as seen from (3.7), $K_-(x;L)$ is given by

$$K_-(x;L) = K(x/\sqrt{2}, x/\sqrt{2}; L) . \tag{6.2}$$

Equation (6.1) is simply the diffusion equation on a half line with a Dirichlet boundary condition and can therefore easily be solved using the Fourier sine transform with respect to the x variable from which it follows that

$$K(x,x_0,t) = \frac{2}{\pi} \int_0^\infty dk e^{-(1/2)k^2 t} \sin(kx) \sin(kx_0)$$

$$= \frac{1}{\sqrt{2\pi t}} \{ e^{-(x-x_0)^2/2t} - e^{-(x+x_0)^2/2t} \} \tag{6.3}$$

and therefore

$$K_-(x;L) = \frac{1}{\sqrt{2\pi L}} (1 - e^{-x^2/L}) . \tag{6.4}$$

One can check, using asymptotic formulas for Airy functions [24] and then replacing the sum in (3.12) by a Riemann integral, that the limit of $h \to 0^+$ of (3.12) coincides exactly with (6.4).

The first term on the right-hand side of (6.4) will remain after the limit $x \to \infty$ is taken and is therefore truncated away before contributing to $u_2(x)$. Hence type $\mathcal{A}$ bubbles give a contribution to $u_2(x)$ going like $\exp(-x^2/L)$ at $h=0$ whereas type $\mathcal{B}$ gives contributions of the form $\exp(-\kappa x)$ and are therefore *highly* dominant over type $\mathcal{A}$ contributions.

B. Type $\mathcal{B}$ bubbles

Now that it has been ascertained that only type $\mathcal{B}$ bubbles need be considered in the calculation of the pair-energy-density correlation function at $h=0$, we can proceed to evaluate them. Before doing so, it should be stressed that, due to additional symmetry at $h=0$ not present when $h>0$, we need to treat $h=0$, hereafter denoted as case (i), and the limit of $h\to 0^+$ of the type $\mathcal{B}$ calculation of Sec. IV, denoted case (ii), as distinct cases.

For convenience, we present the results in this section directly in terms of two-particle wave functions without going to center-of-mass and relative coordinates. As previously stated, the results will only apply to the pair-energy-density correlation function where $U_0=4\tau^2$. Equations (4.1) and (4.2) can be expressed in spectral form as

$$u_2(x;h\,|\mathcal{B})=4\tau^2 e^{-2x}\sum_{\mathbf{n}}|\psi_{\mathbf{n}}(0,y_0)|^2 e^{-E_{\mathbf{n}}(2)x}\ , \tag{6.5}$$

where the eigenstates are labeled by pairs of integers $\mathbf{n}=(n_1,n_2)$ and the two-particle eigenfunctions $\psi_{\mathbf{n}}(y_1,y_2)$ and eigenvalues $E_{\mathbf{n}}(2)$ are given by the Schrödinger equation

$$\left\{-\frac{1}{2}\left[\frac{\partial^2}{\partial y_1^2}+\frac{\partial^2}{\partial y_2^2}\right]+h(y_2-y_1)\right\}\psi_{\mathbf{n}}(y_1,y_2) =E_{\mathbf{n}}(2)\psi_{\mathbf{n}}(y_1,y_2)\ . \tag{6.6}$$

When either $h=0$ or $h\to 0^+$, Eq. (6.6) will have scattering-state solutions of Bethe ansatz type. In addition, the noncrossing constraint on the particle world lines simply that $\psi_{\mathbf{n}}(y,y)=0$ for all y so that $\psi_{\mathbf{n}}(y_1,y_2)$ can be expressed as a Slater determinant

$$\psi_{\mathbf{n}}(y_1,y_2)=\frac{1}{\sqrt{2}}\begin{vmatrix}\varphi_{n_1}(y_1) & \varphi_{n_1}(y_2)\\ \varphi_{n_2}(y_1) & \varphi_{n_2}(y_2)\end{vmatrix}\ , \tag{6.7}$$

where $\varphi_n(y)$ are single-particle wave functions

$$\varphi_{n_j}(y)=\frac{1}{\sqrt{L}}e^{i\omega_j y} \tag{6.8}$$

for $j=1,2$, normalized on a cylinder of period L. The wave numbers $\omega_j=\omega_j(n_j)$ are quantized in terms of the integers n_j. Clearly, the two-particle eigenvalues are given by

$$E_{\mathbf{n}}(2)=\tfrac{1}{2}(\omega_1^2+\omega_2^2)\ . \tag{6.9}$$

Additional symmetries are required to determine the quantization conditions on the wave numbers ω_j and these will differ for the two cases, which we now treat in turn.

Case (i): $h=0$. For this case, the two particles, moving on the cylinder, are effectively indistinguishable. This means that the system is invariant under the mapping

$$Q:\ (y_1,y_2)\mapsto(y_2,y_1+L) \tag{6.10}$$

rather than just being periodic under mapping P of (4.3), although note that $Q^2=P$. Hence, imposing $\psi_{\mathbf{n}}(y_1,y_2)=\psi_{\mathbf{n}}(y_2,y_1+L)$, for all y_1 and y_2, on (6.7) and (6.8) implies that $\omega_j\in\Omega_L^+$ for both $j=1,2$ where here, and in what follows below, we define

$$\Omega_L^{\pm}=\{\omega\in\mathbb{R}:\ e^{i\omega L}=\mp 1\}\ , \tag{6.11}$$

which is consistent with the notation for even (Ω_L^+) and odd (Ω_L^-) parity states in the corresponding planar Ising model. Indeed, note that

$$\psi_{\mathbf{n}}(y_1,y_2)=\pm\psi_{\mathbf{n}}(y_2,y_1+L)\Longleftrightarrow\text{both }\omega_1,\omega_2\in\Omega_L^{\pm}\ . \tag{6.12}$$

So for case (i), just as in the exact Ising model [22], only states in Ω_L^+ contribute to the pair-energy-density correlation function. Putting all this together, we can express the pair-energy-density correlation function $u_2(x\,|\mathcal{B})$ in terms of "single-particle contractions," defined by

$$T_L^{\pm}(x,y)=\frac{2\tau}{L}\sum_{\omega\in\Omega_L^{\pm}}e^{-x(1+\omega^2/2)}e^{iy\omega} \tag{6.13}$$

such that for case (i)

$$u_2(x;h=0|\mathcal{B})=[T_L^+(x,0)]^2-T_L^+(x,y_0)T_L^+(x,-y_0)\ . \tag{6.14}$$

Equation (6.14) has been presented in a short Letter elsewhere [22] (but without the detailed derivation given here) and, for large values of x and L with $x\gg L$ (where the *nonrelativistic* approximation works best), is known to give a reasonable approximation to the exact Ising result [22]. Note, in particular, that at $h=0$ successive eigenvalues are separated by an amount of the order of $1/L^2$.

Case (ii): $h\to 0^+$. Whenever a *nonzero* field is present, any symmetry transformation of the particles has to preserve y_2-y_1. This will, of course, *exclude* the mapping Q. In fact, the appropriate periodicity mapping for this case is P [given by (4.3)], as already used throughout Sec. IV. Thus one would *not* expect the $h\to 0^+$ limit of the results of Sec. IV to coincide with the $h=0$ result of case (i) above because the wave numbers ω_j will be quantized by a different rule. To be more concrete, applying the periodicity P to the wave function given by (6.7) and (6.8), i.e., $\psi_{\mathbf{n}}(y_1,y_2)=\psi_{\mathbf{n}}(y_1+L,y_2+L)$, implies that *either* both $\omega_1,\omega_2\in\Omega_L^+$ *or* both $\omega_1,\omega_2\in\Omega_L^-$. Hence, putting this into Eqs. (6.5) and (6.7)–(6.9) gives

$$\lim_{h\to 0^+}u_2(x;h\,|\mathcal{B}) =\tfrac{1}{2}\sum_{\epsilon=\pm}\{[T_L^{\epsilon}(x,0)]^2-T_L^{\epsilon}(x,y_0)T_L^{\epsilon}(x,-y_0)\} \tag{6.15}$$

for case (ii), where the prefactor of $\frac{1}{2}$ is needed to prevent double counting of states. As expected, Eq. (6.15) is exactly reproduced by taking the $h\to 0^+$ limit of the results of Sec. IV, namely, (4.20), where $K_+(x;L)$ is, of course, independent of h so that one merely has to apply this limit to $m_n(h;L)$ and $p_n(h;L)=4\tau^2|\varphi_n^-(y_0/\sqrt{2})|^2$. Using asymptotic formulas for the modulus-and-phase representation of the Airy functions [24] appearing in (4.18) and (4.19), one finds that

$$M_n(z)\approx n^2\pi^2/z^2 \tag{6.16}$$

as $z \to 0$ while

$$\lim_{h \to 0^+} \varphi_n^-(y_-) = \left[\frac{2\sqrt{2}}{L} \right]^{1/2} \sin(\omega_n^- y_-) , \tag{6.17}$$

where $\omega_n^- = n\pi\sqrt{2}/L$ and, in both (6.16) and (6.17), $n = 1,2,3, \ldots$. Putting all this into (4.20) gives precisely (6.15), after transforming the summation variables to $\omega_1 = (\omega_n^+ - \omega_m^-)/\sqrt{2}$ and $\omega_2 = (\omega_n^+ + \omega_m^-)/\sqrt{2}$ where it is recalled that ω_n^+, defined just after (4.11), is the summation variable for $K_+(x;L)$.

The discrepancy between $h = 0$ and $h \to 0^+$ does *not*, of course, necessarily mean that the energy-density-correlation function itself has a jump discontinuity in h at $h = 0$ for finite L. In any case, when $h > 0$, type $\mathcal{A}$ bubbles dominate for $0 < h < h_\times$ and thus will always dominate for small enough *nonzero* h. Hence $u_2(x;h|\mathcal{A})$ rather than $u_2(x;h|\mathcal{B})$ will describe $u_2(x)$ for very small positive h *except* when $h_\times \to 0$ in addition to $h \to 0^+$ while keeping $h > h_\times$. Having $h_\times \to 0$ means that $L \to \infty$ and we know that $u_2(x;h)$ is continuous in h in the limit $L \to \infty$ or, more specifically, $u_2(x;h|\mathcal{B})$, as given by (4.20), in the limit $h^{1/3}L \to \infty$. Furthermore, one can see by taking the limit of $L \to \infty$ on expressions (6.14) and (6.15) that the discrepancy between $u_2(x;h=0|\mathcal{B})$ and $\lim_{h \to 0^+} u_2(x;h|\mathcal{B})$ *vanishes* in the bulk since $\lim_{L \to \infty} T_L^-(x,y) = \lim_{L \to \infty} T_L^+(x,y)$.

Further insight into this discrepancy can be gained by expressing $T_L^\pm(x,y)$ in terms of *windings* of particle paths around the cylinder as was similarly done in Sec. IV A and Ref. [22]. Using the Poisson summation formula, Eq. (6.13) can be rewritten as

$$T_L^\pm(x,y) = \tau \left[\frac{2}{\pi x} \right]^{1/2} e^{-x} \sum_{n=-\infty}^{\infty} (\mp 1)^n e^{-(y+nL)^2/2x} , \tag{6.18}$$

where the summation index n refers to the winding number of the particle paths as they encircle the cylinder (i.e., homotopy class). Substituting $T_L^+(x,y)$, given by (6.18), into (6.14) one sees that, for case (i), the first finite-size correction to the bulk $L \to \infty$ limit of $u_2(x|\mathcal{B})$ comes from one side of the bubble winding around once (winding number $n = 1$) while the other does not wind at all (winding number $n = 0$), as illustrated in Fig. 6. Note that domain-wall configurations of the type shown in Fig. 6 divide the cylinder into just two regions of opposite magnetization—a situation not allowed when h is *nonzero*. For case (ii), one sees that when substituting $T_L^\pm(x,y)$, given by (6.18), into (6.15), the terms corresponding to the configuration in Fig. 6 for $\epsilon = +$*cancel* with those for $\epsilon = -$ due to the $(\mp 1)^n$ term in (6.18). Hence, as required for nonzero h, configurations of this type do *not* occur for case (ii) and the first finite-size correction to the bulk form of $u_2(x|\mathcal{B})$ comes from winding configurations of the type shown in Fig. 5, where both sides of the bubble wind around once.

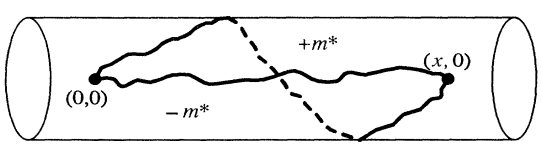

FIG. 6. Depiction of a bubble configuration (type $\mathcal{B}$) occurring at $h = 0$ only, where one side winds around once while the other does not wind at all. Note that it divides the cylinder into just *two* domains, *not* three as in Fig. 5.

So, to conclude, it should be emphasized that to determine the behavior of $u_2(x)$ at $h = 0$, one sums over bubbles of type $\mathcal{B}$ but, due to the higher symmetry, the procedure set out under case (i) must be followed, which is quite different from taking the limit of $h \to 0^+$ of the results of Sec. IV, i.e., case (ii).

As a further illustration of the importance of boundary conditions on the spectral form of correlation functions, we consider $u_2(x)$ at $h = 0$ for another geometry. Instead of a cylinder of period L, we now take a strip of infinite length but with a finite width L. The Ising lattice is confined between the two edges $y = \pm L/2$ along which the Ising spins are forced to be up. The exact Ising analysis for this case was carried out by Abraham and Martin-Löf [25]. The corresponding bubble model for this consists of the bubble as before but with sides confined to lie within $|y| < L/2$ rather than lying on the cylinder. Hence $u_2(x)$ is given by Eq. (6.5) with the eigenstates given by Eq. (6.6) for $h = 0$, but now $|y| \le L/2$ and the boundary conditions are $\psi_n(-L/2, y_2) = \psi_n(y_1, L/2) = 0$, i.e., that of two noncrossing particles in an infinite square well. The eigenfunctions are still written in Slater form (6.7) with the same eigenvalues $E_n(2)$ as in (6.9) but with different $\varphi_{n_j}(y)$ for $j = 1,2$ given by

$$\varphi_{n_j}(y) = \left[\frac{2}{L} \right]^{1/2} \sin[\omega_j(y + L/2)] \tag{6.19}$$

being normalized single-particle wave functions on a strip of width L having $\varphi_{n_j}(\pm L/2) = 0$. Thus the wave numbers $\omega_j = \omega_j(n_j)$ are quantized through

$$\omega_j = n_j \pi / L, \quad n_j = 1,2,3, \ldots \tag{6.20}$$

for $j = 1,2$. Note that this quantization of ω_j is *distinct* from the above cylinder results for both case (i) and case (ii). In the exact Ising model, the wave-number spectrum is quantized according to a more complicated rule [25] (involving Onsager's hyperbolic triangle [7]), which limits to that given by (6.20) for *large* L (and sufficiently small n_j so that ω_j stays small). Hence, as in the cylinder result at $h = 0$, substituting (6.19), with (6.20), into Eqs. (6.5) and (6.7) gives a $u_2(x)$ that compares well with the exact Ising model for large x and L with $x \gg L$.

VII. CONCLUSION

In this paper we have demonstrated the extent to which the structure of the two-point function for a subcritical Ising model [or a model with a similar O(1) sym-

metry], with a bulk symmetry-breaking field H on a lattice wrapped on a cylinder of finite circumference M, can be understood in terms of a simple coarse-grained description taking into account important domain-wall fluctuations only, namely, the *bubble model.*

This approach gives rise to a correlation function whose field and finite-size dependence is consistent with earlier studies, particularly those based on an analysis of the transfer-matrix spectrum [1–5]. The important crossover behavior in the mass gap of this spectrum at $H=H_\times$, coming from an avoided-level-crossing effect, is recaptured within the bubble phenomenology, coming from a radical change in the form of the dominant bubbles contributing to the correlation function. According to the bubble model, the correlation function itself takes a significantly different functional form at each side of $H_\times$. Previous transfer-matrix work [1,4,5] suggests that the crossover field $H_\times$ depends on M like $H_\times \propto 1/M$. The bubble model confirms this to leading order for large M but adds algebraic corrections to this, the first one going like $1/M^{5/3}$. The bubble model can be formulated using scale-free variables, which is particularly useful in the critical region. Thus, near the critical point, the equation $H_\times = H_\times(M,T)$ can be expressed in a scaled homogeneous form. Applying the bubble model *at* $H=0$ gives results that compare very well with exact analysis of the Ising model.

ACKNOWLEDGMENTS

The authors thank the Engineering and Physical Sciences Research Council (United Kingdom) for financial support under Grants Nos. GR/H73028, B/92/AF/1446, B/92/RF/1420, and B/94/AF/1769.

APPENDIX: ASYMPTOTIC FORM OF $K_-(x;L)$ (TYPE $\mathcal{A}$)

Here we give details of the asymptotic calculation carried out in Sec. III A, namely, how the asymptotic expression of $K_-(x;L)$ (type $\mathcal{A}$) for large $h^{1/3}x$, given by (3.13), follows from the spectral series in Eq. (3.12). We use Laplace's method applied to the sum in (3.12), which starts from the assertion that for large $h^{1/3}x$, the sum is dominated by terms peaked around the maximum one. Since $a_n \to -\infty$ as $n\to\infty$, $\mathrm{Ai}^2(h^{1/3}x+a_n)$ will eventually peak at a large value of n corresponding to a negative value of $h^{1/3}x+a_n$ no matter how large (and positive) $h^{1/3}x$ is. However, the factor $\exp(h^{2/3}La_n)$ in the summand will serve to suppress the large n terms provided $h^{2/3}L$ is sufficiently large. Thus we assume by ansatz that as $h^{1/3}x\to\infty$ and $h^{2/3}L\to\infty$, the maximum term will occur at an n that is *large* but still keeps $h^{1/3}x+a_n$ *large and positive.* Hence we substitute the standard asymptotic expressions [24]

$$\mathrm{Ai}(h^{1/3}x+a_n)\approx \frac{\exp[-\frac{2}{3}(h^{1/3}x+a_n)^{3/2}]}{2\pi^{1/2}(h^{1/3}x+a_n)^{1/4}}\ , \tag{A1}$$

$$a_n \approx -(3\pi n/2)^{2/3}\ , \tag{A2}$$

$$[\mathrm{Ai}'(a_n)]^2 \approx \pi^{-1}(3\pi n/2)^{1/3} \tag{A3}$$

into the sum (3.12) and then approximate it by a Riemann integral (for large x) taking $u=3\pi n/2x$ as the integration variable. By changing the integration variable to $v=u^{2/3}$ we find that as $h^{2/3}x$ gets large,

$$K_-(x;L)\approx \frac{\sqrt{2}(hx)^{1/3}}{4\pi}\int_0^\infty dv \frac{\exp[-x^{2/3}\Phi(v)]}{[(hx)^{1/3}-v]^{1/2}}\ , \tag{A4}$$

where

$$\Phi(v)=\tfrac{4}{3}x^{1/3}[(hx)^{1/3}-v]^{3/2}+h^{2/3}Lv\ . \tag{A5}$$

Laplace's method is now applied to (A4), where, as $x\to\infty$, the integral is dominated by the region around v_0, the minimum of $\Phi(v)$. Thus $\Phi'(v_0)=0$ implies that

$$v_0=(hx)^{1/3}\left[1-\frac{hL^2}{4x}\right]\ . \tag{A6}$$

Note that the integrand in (A4) has a branch point at $v=(hx)^{1/3}$. However, in order to be consistent with the above ansatz that the argument of $\mathrm{Ai}(h^{1/3}x+a_n)$ be large and positive at the maximum of the summand, it is required that $v_0<(hx)^{1/3}$ [as is satisfied by (A6)] and that $h^{2/3}L$ be large (as anticipated). We also require that v_0 lie within the range of integration, i.e., $v_0>0$, which implies that we must have

$$x > hL^2/4\ . \tag{A7}$$

Hence, from Laplace's method, as $x\to\infty$,

$$\int_0^\infty dv \frac{\exp[-x^{2/3}\Phi(v)]}{[(hx)^{1/3}-v]^{1/2}} \approx \left[\frac{2\pi}{x^{2/3}\Phi''(v_0)}\right]^{1/2}\frac{\exp[-x^{2/3}\Phi(v_0)]}{[(hx)^{1/3}-v_0]^{1/2}} \tag{A8}$$

so that, from (A4)–(A6),

$$K_-(x;L)\approx \frac{\exp[-x^{2/3}\Phi(v_0)]}{\sqrt{2\pi L}}\ , \tag{A9}$$

where

$$x^{2/3}\Phi(v_0)=hLx-\tfrac{1}{12}h^2L^3\ , \tag{A10}$$

giving (3.13) of Sec. III A.

[1] V. Privman and M. E. Fisher, J. Stat. Phys. **33**, 385 (1983).
[2] C. M. Newman and L. S. Schulman, J. Math. Phys. **18**, 23 (1977).
[3] R. J. McCraw and L. S. Schulman, J. Stat. Phys. **18**, 293 (1978).
[4] V. Privman and L. S. Schulman, J. Phys. A **15**, L231 (1982).
[5] V. Privman and L. S. Schulman, J. Stat. Phys. **29**, 205

(1982).
[6] At $H=0$, if $\mathcal{O}(X,Y)$ is the bond energy, the matrix element will be zero [in which case $1/\xi=\beta M(f_2-f_0)$] whereas for spins it stays nonzero.
[7] L. Onsager, Phys. Rev. **65**, 117 (1944).
[8] M. E. Fisher, J. Phys. Soc. Jpn. Suppl. **26**, 87 (1969).
[9] C. N. Yang, Phys. Rev. **85**, 808 (1952).
[10] M. E. Fisher and W. J. Camp, Phys. Rev. Lett. **26**, 565 (1971).
[11] B. M. McCoy and T. T. Wu, Phys. Rev. D **18**, 1259 (1978).
[12] D. B. Abraham, Phys. Rev. Lett. **50**, 291 (1983).
[13] M. E. Fisher, J. Stat. Phys. **34**, 667 (1984).
[14] D. B. Abraham and P. J. Upton, Phys. Rev. Lett. **69**, 225 (1992).
[15] D. B. Abraham and P. J. Upton, Int. J. Mod. Phys. C **3**, 1071 (1992).
[16] D. B. Abraham and P. J. Upton, Phys. Rev. Lett. **70**, 1567 (1993).
[17] D. B. Abraham, N. M. Švrakić, and P. J. Upton, Phys. Rev. Lett. **68**, 423 (1992).
[18] Here we assume that the surface tension and correlation length are isotropic, as would be the case for temperatures sufficiently close to the critical point. For temperatures further below, one would have to take into account lattice anisotropy so that the surface tension would be angle dependent, i.e., $\tau=\tau(\theta)$. In this case, distances in the Y direction would be rescaled in terms of the "surface stiffness" $\tilde{\Sigma}=\tau(0)+\tau''(0)$ [D. S. Fisher, M. P. A. Fisher, and J. D. Weeks, Phys. Rev. Lett. **48**, 369 (1982)], which would also enter into the definition of the rescaled field h.
[19] G. Wulff, Z. Kristallogr. **34**, 449 (1901).
[20] D. B. Abraham and E. R. Smith, Phys. Rev. B **26**, 1480 (1982).
[21] D. B. Abraham and E. R. Smith, J. Stat. Phys. **43**, 621 (1986).
[22] D. B. Abraham, D. O'Connor, A. O. Parry, and P. J. Upton, Phys. Rev. Lett. **73**, 1742 (1994).
[23] D. B. Abraham and P. J. Upton (unpublished).
[24] H. A. Antosiewicz, in *Handbook of Mathematical Functions*, edited by M. Abramowitz and I. A. Stegun (Dover, New York, 1965), Chap. 10.
[25] D. B. Abraham and A. Martin-Löf, Commun. Math. Phys. **32**, 245 (1973).